Journal of Biomolecular Structure and Dynamics

ISSN: (Print) (Online) Journal homepage: https://www.tandfonline.com/loi/tbsd20

Identification of novel potential inhibitors of varicella-zoster virus thymidine kinase from ethnopharmacologic relevant plants through an *in-silico* approach

Samuel Kojo Kwofie, Dorothy Gyamfua Annan, Cynthia Ayefoumi Adinortey, Daniel Boison, Gabriel Brako Kwarko, Rachel Araba Abban & Michael Buenor Adinortey

To cite this article: Samuel Kojo Kwofie, Dorothy Gyamfua Annan, Cynthia Ayefoumi Adinortey, Daniel Boison, Gabriel Brako Kwarko, Rachel Araba Abban & Michael Buenor Adinortey (2021): Identification of novel potential inhibitors of varicella-zoster virus thymidine kinase from ethnopharmacologic relevant plants through an *in-silico* approach, Journal of Biomolecular Structure and Dynamics, DOI: 10.1080/07391102.2021.1977700

To link to this article: https://doi.org/10.1080/07391102.2021.1977700

JOURNAL OF BIOMOLECULAR STRUCTURE AND DYNAMICS
https://doi.org/10.1080/07391102.2021.1977700

Identification of novel potential inhibitors of varicella-zoster virus thymidine kinase from ethnopharmacologic relevant plants through an *in-silico* approach

Samuel Kojo Kwofie[a,b], Dorothy Gyamfua Annan[b], Cynthia Ayefoumi Adinortey[c], Daniel Boison[d], Gabriel Brako Kwarko[b], Rachel Araba Abban[b] and Michael Buenor Adinortey[d]

[a]Department of Biomedical Engineering, School of Engineering Sciences, College of Basic and Applied Sciences, University of Ghana, Accra, Ghana; [b]West African Centre for Cell Biology of Infectious Pathogens, Department of Biochemistry, Cell and Molecular Biology, College of Basic and Applied Sciences, University of Ghana, Accra, Ghana; [c]Department of Molecular Biology and Biotechnology, School of Biological Sciences, University of Cape Coast, Cape Coast, Ghana; [d]Department of Biochemistry, School of Biological Sciences, University of Cape Coast, Cape Coast, Ghana

Communicated by Ramaswamy H. Sarma

ABSTRACT

Although Varicella or chickenpox infection which is caused by the varicella-zoster virus (VZV) has significantly been managed through vaccination, it remains an infection that poses threats to the nearest future due to therapeutic drawbacks. The focus of this research was geared towards *in silico* screening for the identification of novel compounds in plants of ethnopharmacological relevance in the treatment of chicken pox in West Africa. The work evaluated 65 compounds reported to be present in *Achillea millefolium, Psidium guajava* and *Vitex doniana sweet* to identify potential inhibitors of thymidine kinase, the primary drug target of varicella zoster virus. Out of the 65 compounds docked, 42 of these compounds were observed to possess binding energies lower than −7.0 kcal/mol, however only 20 were observed to form hydrogen bond interactions with the protein. These interactions were elucidated using LigPlot^{+} and MM-PBSA analysis with residue Ala134 predicted as critical for binding. Pharmacological profiling predicted three potential lead compounds comprising myricetin, apigenin- 4′ -glucoside and Abyssinone V to possess good pharmacodynamics properties and negligibly toxic. The molecules were predicted as antivirals including anti-herpes and involved in mechanisms comprising inhibition of polymerase, ATPase and membrane integrity, which were corroborated previously in other viruses. These drug-like compounds are plausible biotherapeutic moieties for further biochemical and cell-based assaying to discover their potential for use against chickenpox.

Abbreviations: ADMET: absorption, distribution, metabolism, excretion and toxicity; AUC: Area Under Curve; CYP: Cytochromes P_{450}; DUD-E: Directory of Useful (Docking) Decoys- Enhanced; DUD-E: Database of Useful (Docking) Decoys - Enhanced =; ESOL: Effective Solubility; GROMACS: GROningen MAchine for Chemical Simulations; HPC: High Performance Computing; ID: Identification; Log P: Logarithm of the octan-1-ol/water partition coefficient; MD: Molecular Dynamics; MM-PBSA: Molecular Mechanics Poisson Boltzmann Surface Area; MW: Molecular Weight; P-gp: Permeability glycoprotein; PASS: Prediction of Activity Spectra for Substance; PDB: Protein Data Bank; RCSB: Research Collaboratory for Structural Bioinformatics; Rg: radius of gyration; RMSD: Root Mean Square Deviation; RMSF: Root Mean Square Fluctuation; ROC: Receiver Operating Characteristic; SDF: Structure Data File; SMILES: Simplified Molecular Input Line Entry System; TK: thymidine kinase; TPSA: Topological Polar Surface Area; UFF: Universal Force Field; VZV: varicella-zoster virus

ARTICLE HISTORY
Received 25 February 2021
Accepted 3 September 2021

KEYWORDS
Chickenpox; varicella zoster virus; thymidine kinase; molecular docking; molecular dynamics simulations

1. Introduction

Many viral infections associated with children include varicella or varicella-zoster, usually known as chickenpox infection. Though this viral disease is mostly found in juveniles, there are reports of its occurrence among adults (Civen et al., 2009; Marin et al., 2008; Singh et al., 2015). Varicella is a well-recognized systemic highly contagious airborne disease caused by varicella zoster virus (VZV), a virus in the *Herpesviridae* family that also causes shingles. The virus can also be transmitted via fomites from skin lesions present in chicken pox and shingles (Andrei & Snoeck, 2011). Humans become infected with the varicella zoster virus when the virus gets in contact with either the mucosa of the upper respiratory tract or conjunctiva (Cohen et al., 1999). With an incubation period of 14 days, the virus circulates through the bloodstream to the skin in mononuclear cells, which causes the vesicular rash associated with the infection (Cohen et al., 1999). Chickenpox is characterized by fever and may be intricate with secondary bacterial infections such as cellulitis and necrotizing fasciitis, common among adults, adolescents and immunocompromised individuals (Gershon, 2017). Following

CONTACT Michael B. Adinortey madinortey@ucc.edu.gh Department of Biochemistry, University of Cape Coast, Cape Coast, Ghana.
Supplemental data for this article can be accessed online at https://doi.org/10.1080/07391102.2021.1977700

primary infection, VZV establishes latency in the sensory ganglia which can reactivate to cause shingles (herpes zoster) (Andrei & Snoeck, 2011). Chickenpox can be complicated by chronic pain and other serious neurological and oracular disorders like vasculopathy, keratitis, and retinopathy as well as multiple visceral and gastrointestinal disorders including peptic ulcers, hepatitis and pancreatitis (Angamuthu et al., 2019).

Vaccines are available in many countries to prevent the onset of disease (Baxter et al., 2013; Park et al., 2013) include Varilrix® and Varivax® (Floret, 2005; Heininger & Seward, 2006). Apart from vaccination existing for chickenpox infection, the condition is usually managed with some orthodox pharmacotherapeutic agents, which are usually antiviral nucleoside analogues that require *in vivo* phosphorylation by thymidine kinase (TK). For many years, acyclovir® has been the mainstay for the treatment of varicella infection, however other antiviral agents such as valacyclovir and famciclovir have been developed to overcome the low oral bioavailability of acyclovir and provide a more effective regimen (Balfour et al., 2001; Chou & Lurain, 2019). The downside of the use of these antivirals is the adverse side effects such as headache, vomiting, neurotoxic psychological effects, and renal dysfunction (Chou & Lurain, 2019). These therapeutic shortfalls warrant more research in the drug discover pipeline to identify potent alternatives with less adverse effects.

An essential drug target for this viral infection is varicella zoster virus thymidine kinase. The thymidine kinase is a phosphotransferase enzyme present in most living cells, responsible for catalyzing the transfer of phosphate groups from ATP to deoxythymidine to form deoxythymidine monophosphate (Hoffmann et al., 2017). The thymidine kinase is a protein encoded by the varicella zoster virus that has both thymidine and thymidylate phosphorylating activities (Hoffmann et al., 2017). The protein is involved in the replication of the viral DNA making it integrally involved in host cellular infection mechanisms. Most drugs that are used against the varicella infection act competitively with the viral nucleoside triphosphates, mostly thymidine triphosphates, in order to terminate the replication of the virus (Topalis et al., 2018). Acyclovir, for instance is first phosphorylated selectively by the viral thymidine kinase protein to form its monophosphate derivative, which is further metabolized by the host cellular enzymes to form the triphosphate derivatives. These then act as preferred substrates for the viral DNA polymerase and disrupt the DNA synthesis in the virus thereby terminating its activity (Chou & Lurain, 2019).

Plants have served as a major reservoir of medicine for numerous diseases including viral infections. They are recognized as natural sources for the synthesis of medicinal compounds, and the characterization of these compounds have directed the discovery of new and economical drugs that have curative and prophylactic potentials (Huie, 2002). According to World Health Organization, approximately 60% – 80% of the world population depends on medicinal plants for their primary healthcare, and most drugs are derived from unmodified natural products or semi-synthetic drugs obtained from natural sources (Mothana et al., 2010; W.H.O, 2002). The bioactivity of natural products is due to the presence of certain compounds or secondary metabolites often produced by these plants to serve as defense against herbivory, pathogen attack, abiotic stress and also inter plant competition (Mothana et al., 2010). Among the many plants used in the treatment of chickenpox in West Africa are *Psidium guajava* (Ayitey-Smith, 1989), *Vitex doniana* sweet (Jean et al., 2019) and *Achillea millefolium* (Bonsu, 2012).

Psidium guajava commonly called guava, is a plant that is known due to its curative potentials especially as an antidiarrheal agent as well as to treat stomach aches that arises as a result of indigestion (Gutierrez et al., 2008). This plant has also been reported to be used for the treatment of chicken pox (Ayitey-Smith, 1989). *Psidium guajava* is a plant that grows in all subtropical and tropical area, and has the ability to adapt to various climatic conditions, although it prefers to grow in dry climates (Gutierrez et al., 2008). It belongs to the family *Myrtaceae* and grows about 10 m high possessing a thin, but smooth, patchy and peeling bark (Gutierrez et al., 2008). Several bioactive compounds reported to be isolated from *Psidium guajava*, are responsible for its wide use as a treatment for several infections. Some of these compounds include guajanerin, avicularin, kaemferol, myricetin, mecocyanin, quercetin, leucocyanidin, guavin B, chlorogenic acid, limonene, cuproel, caryophyllene, copaene, and zulene (Gutierrez et al., 2008).

Another commonly used plant in the treatment of chicken pox in some West African countries is *Vitex doniana* sweet (Ayitey-Smith, 1989; Bonsu, 2012; Jean et al., 2019). *Vitex doniana* sweet can be said to be one of the most abundant tree species usually found in Savannah regions of the world (Leakey, 2001). It is a multiple-use plant with both nutritional and medicinal importance (Eyog Matig et al., 2002). The fruit of the plant is edible while the other parts are used as medicine in the treatment of ulcer, diabetes, and edema (Osuagwu & Eme, 2013). It belongs to the family *Verbenaceae* and grows up to about 25 m (Osuagwu & Eme, 2013). Bioactive compounds isolated from *Vitex doniana Sweet* include cupreol, campesterol, ecdysteron, loliolide, 4- pinoresinol, chrysin, Abyssinone V, galangin and catechol (Ajiboye, 2015).

Achillea millefolium commonly known as yarrow, is another medicinal plant which is used to manage viral infections and related diseases including chicken pox (Bonsu, 2012). It belongs to the *Asteraceae* family (Benedek & Kopp, 2007). Traditionally, the yarrow plant is used for the treatment of inflammation and also for spasmodic gastrointestinal disorders and hepatobiliary complaints (Benedek & Kopp, 2007). In addition, it is also used as an appetite enhancing drug, wound healing and against skin inflammations. Apart from the traditional uses, the yarrow plant is also contained in various industrial tea mixtures and other phytopharmaceuticals (Benedek & Kopp, 2007). Several bioactive compounds have been isolated from different parts of yarrow. These bioactive compounds include butain, choline, betanocine, achilletin and azulene (Applequist & Moerman, 2011; Chandler et al., 1982)

Several cheminformatics studies have identified inhibitors against viral drug targets (Kadioglu et al., 2021; Kwofie,

Broni, et al., 2019; Kwofie et al., 2021; Prasanth et al., 2020; Yaeghoobi et al., 2016). The structure of the varicella zoster virus thymidine kinase has been solved using X-ray crystallography and modelled using homology modeling, as well as molecular docking studies have been undertaken (Abo Almaali, 2018; Bird et al., 2003; Spadola et al., 2003).

In silico pharmacological screening of isolated compounds of *Psidium guajava, Vitex doniana Sweet* and *Achillea millefolium* plants used for the treatment of chickenpox could contribute to identifying novel VZV thymidine kinase inhibitors of natural origin. Even though, many compounds have been isolated from these plants, there is dearth of literature pertaining to their pharmacological utility with regards to chicken pox. Therefore, this work used cheminformatics approaches including molecular docking and dynamics simulation to screen bioactive constituents present in different extracts of these plants against the drug target VZV-thymidine kinase. In addition, it explored the propensity of the potential novel leads to inhibit viral replication in chickenpox. The study also elucidated new insights into the binding mechanisms and identified residues critical to interactions as well as for design of next-generation anti-VZV molecules. More so, this work identified mechanisms of actions and biological activity of identified natural products.

2. Materials and methodology

The methodology schema describing the step-by-step techniques used for the study is described (Figure 1). The work involved the generation of the library from ethnopharmacological plants which were screened against VZV Thymidine Kinase Receptor to identify potential leads using cheminformatics.

2.1. Pre-processing of VZV thymidine kinase receptor

The 3 D crystal structural of VZV thymidine kinase with resolution of 3.2 Å was retrieved from Protein Data Bank (www.rcsb.org, PDB ID: 1OSN). The BVDU-MP and ADP ligands as well as all water molecules were detached from the protein structure using PyMol (version 1.7.4.5) (Schrodinger, 2010). SwissPDB viewer (Guex et al., 2009) was used to replace all missing residues before the topology of the protein was generated. The final molecule was then saved in a (.pdb) file for molecular dynamics (MD) simulations. The MD simulations of the receptor were performed using a high-performance computing (HPC) server. The MD was done using the downloaded crystal structure of the receptor by means of GROMACS (Lemkul, 2019). Energy minimization was done at 25,000,000 steps and position restraints were applied to 1OSN, thereafter a temperature equilibration at 300 K followed by a pressure equilibration at 1 bar was carried out for 100 ps each. The production MD was then run for 100 ns, keeping the temperature at 300 K and the pressure at 1 bar. Xmgrace (Turner, 2005) was used to plot the graphs generated from the MD simulations. The final (.gro) file was converted back to (.pdb) file for molecular docking.

2.2. Selection of ligands

A library composed of 65 isolated compounds obtained from *Achillea millefolium*, *Psidium guajava and Vitex doniana* sweet together with 2 known inhibitors of VZV thymidine kinase comprising acyclovir and valacyclovir was generated. These ligands were obtained from PubChem (https://pubchem.ncbi.nlm.nih.gov/) (Kim et al., 2019) and energy minimized using OpenBabel environment via PyRx (Dallakyan & Olson, 2015). The energy minimization was done by means of the Universal Force Field (UFF) (Artemova et al., 2016). The Universal Force Field (UFF) is applicable to almost all atom types of the periodic table and such flexibility makes this force field a potential good candidate for simulations involving a large spectrum of systems (Artemova et al., 2016). This force field is non-reactive, i.e. the topology of the system under study is considered as fixed and no creation or breaking of covalent bonds is possible (Jaillet et al., 2017). The algorithm employed for the energy minimization using OpenBabel environment in PyRx (Dallakyan & Olson, 2015) was the conjugate gradient optimization algorithm, and energy minimization was done for 200 steps, with the number of updates for a step being one and also energy difference for stop being 0.1. All ligands were converted to a (.pdbqt) formats.

2.3. Molecular docking of compounds against VZV thymidine kinase receptor

Known active site residues were selected within a grid box of dimensions X: 58.75 Å, Y: 36.22 Å, and Z: 25 Å; and center X: 49.04 Å, Y: 32.84 Å, and Z: 67.09 Å within AutoDock Vina environment which uses the gradient optimization algorithm (Trott & Olson, 2010). Molecular docking was then carried out to ascertain the binding affinity between the protein and the ligands. The resulting docked poses of the ligands within the protein structure were visualized using PyMol.

2.4. Mechanism of binding characterization

LigPlot^{+} (v1.4.5) (Laskowski & Swindells, 2011; Wallace et al., 1995) was used to characterize the binding mechanisms between the target protein structure and selected compounds based on their hydrogen and hydrophobic interactions.

2.5. Validation of docking protocol

LigAlign (Heifets & Lilien, 2010) was employed in validating the docking protocol. The ligand was removed from the co-crystalized complex and re-docked. The redocked and co-crystallized complexes were superimposed using LigAlign to calculate the deviation between them. LigPlot^{+} was used to obtain co-occurring interaction residues from both complexes for further validation of the docking protocol. The Receiver Operating Characteristic (ROC) curve was plotted *via* easyROC (Goksuluk et al., 2016) and the Area Under Curve (AUC) was subsequently computed. Twelve active

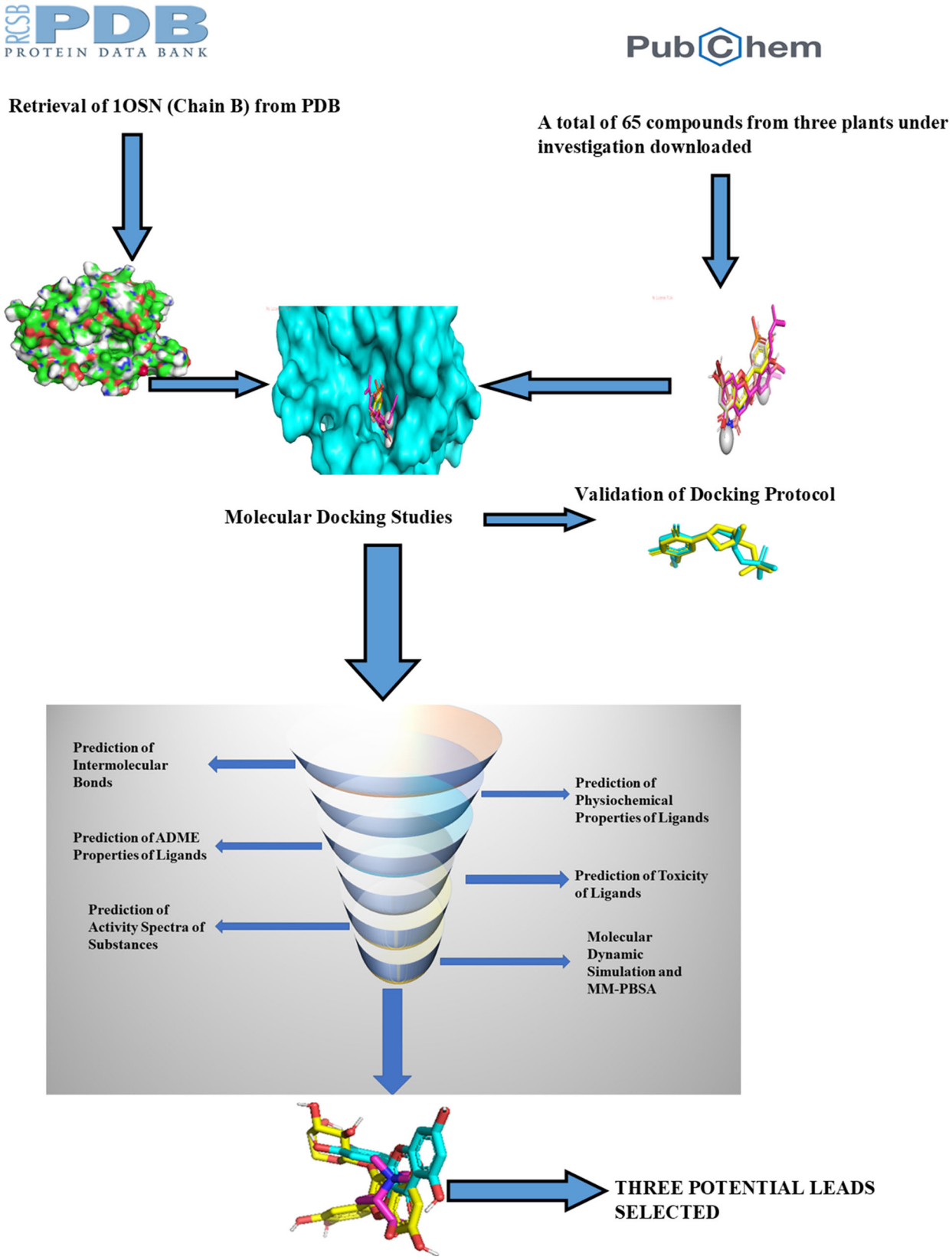

Figure 1. Methodology schema employed in the *In silico* studies for predicting potential anti-VZV thymidine kinase compounds. Natural compounds from three medicinal plants used traditionally in Ghana against chicken pox were downloaded from the PubChem Database and were docked against the VZV thymidine kinase receptor. Compounds with binding affinities of $\leq$-7.0 kcal/mol against the receptor were selected for downstream analysis. The methods include the characterizations of protein-ligand complexes, biological activity predictions and MD simulations.

compounds comprising satabacin, sattazolin, valacyclovir, acyclovir, brivudine, sorivudine, CF-1743, adefovir, cidofovir, penciclovir, 5- bromothienyldeoxyridine and chlorovinyl-deoxyuridine (Migliore, 2010) were used to generate a total of 600 decoys. Each active compound was used to generate 50 decoys *via* the Directory of Useful (Docking) Decoys-

Enhanced (DUD-E) (Mysinger et al., 2012). All the compounds were then docked against the receptor (1OSN).

2.6. MD simulations and MM-PBSA calculations of receptor-ligand complexes

Complexes with optimum binding affinities were further subjected to molecular dynamics simulation to investigate flexibility and stability. All molecular dynamics (MD) simulations were performed for 100 nanoseconds using GROMACS version 2018 with the force field, GROMOS96 43a1 and SPC water model. MDs were carried out on a Dell EMC high performance computing (HPC) system that comprises CentOS 7 operating systems, 6 nodes, 12 GPUs, 216 CPUs and storage of 277 TB, located at the West African Centre for Cell Biology of Infectious Pathogens (WACCBIP), University of Ghana, Accra. The simulations were done in a dodecahedron box of size 1.0 nm, solvated with SPC water and neutralized by adding 4 chlorine ions. For the MD of the docked complex, the topology file for the potential leads, the co-crystallized ligand and the known drug inhibitor, was generated using PRODRG2 server (Schüttelkopf & Van Aalten, 2004) with the settings herein (Chirality: Yes, Charges: Full, EM: No). Energy minimization was done at 50000 steps using the steepest descent algorithm. Position restrains were applied to both the proteins and ligands using the holonomic restrain algorithm, after which a temperature equilibration at 300 K followed by a pressure equilibration at 1 bar was performed for 50,000 ps each. Temperature and pressure coupling were performed with Berenson-thermostat and Parrinello-Rahman barostat, respectively. Particle Mesh Ewald (PME) (Essmann et al., 1995) was used for calculating long-range electrostatics. A short range cut off of 1.0 nm was set for van der Waals interaction. Moreover, time-step value was set to 2 fs. The production MD runs were then performed for 100 ns, keeping the temperature at 300 K and the pressure at 1 bar. Xmgrace (Turner, 2005) was used to plot the graphs generated from the MD simulations.

Molecular Mechanics Poisson Boltzmann Surface Area (MM-PBSA) computations of the complexes were carried out using g_mmpbsa (Kumari et al., 2014) MM-PBSA calculates the binding free energy components and the discrete energy contributions of the residues. This is achieved primarily by using a thermodynamic path that includes solvation (Genheden & Ryde, 2015). Graphs of binding free energies were obtained with the R programming package.

2.7. Pharmacological and toxicity profiling of selected compounds

The pharmacological properties of all the ligands selected were analyzed using the SwissADME (Daina et al., 2017). The compounds were then filtered using the Lipinski's rule of five (Lipinski, 2016), Bioavailability Score (Martin, 2005) and the Veber's rule (Veber et al., 2002). In addition, the pharmacokinetic properties absorption, distribution, metabolism, excretion (ADME) were predicted using SwissADME (Daina et al., 2017). The toxicity of the ligands was predicted using the PKCSM (Pires et al., 2015) (http://biosig.unimelb.edu.au/pkcsm/prediction).

2.8. Prediction of biological activity of selected compounds

Prediction of Activity Spectra for Substance (PASS) (Filimonov et al., 2014) was used for the prediction of the biological activity of selected compounds based on a training dataset of known substrate present in its database. Simplified Molecular Input Line Entry System (SMILES) of the compounds were used as inputs.

3. Results and discussion

The focus of the work was to screen the constituents of three ethnopharmacological plants which are used to treat varicella-zoster virus infections in Ghana against VZV thymidine kinase receptor to identify potential novel bioactive compounds. A total of 65 compounds presents in *Achillea millefolium, Psidium guajava* and *Vitex doniana sweet* plants were used for *in silico* studies. In general, the properties of potential novel lead compounds include low binding energy (high binding affinity) to the target, reasonably good ADMET properties and strong intermolecular interactions between protein receptors and the ligands (Prasanth et al., 2020).

3.1. Molecular docking analysis

The VZV thymidine kinase is observed to be a homo tetrameric protein having its active site present within each subunit and not at the interface of the interacting subunits (Bird et al., 2003). Therefore, it was ideal to select any one of the chains (chain B) of the entire protein for docking analysis. This approach is also seen to be employed in a study that involved identical subunits for docking (Minai-Tehrani et al., 2015). In determining novel potential leads against the VZV thymidine kinase, molecular docking studies was performed using a total of 65 natural products together with two known inhibitors comprising acyclovir and valacyclovir (Arvin, 1996). Ligands possessing binding energies less than −7 kcal/mol were selected for downstream analyses (Prasanth et al., 2020) with a total of 42 complying with this threshold. Details of the binding energies of the ligands with the protein and the biomolecular interactions are described (Table 1 and Supplementary Table 1). Residues comprising Ala20, Tyr21, Gly22, Ile23, Gly24, Thr26, Thr27, Glu48, Trp53, Ile62, Tyr66, Gln90, Phe93, His97, Asp129, Arg130, Ser135, Phe139, Arg143, Arg183 and Pro302 were identified in the active site of the structure of VZV thymidine kinase (Bird et al., 2003), therefore molecular docking of the ligands against the receptor was done in the active site pocket of the protein (Figure 2).

Table 1. Binding energies and molecular interactions of two known inhibitors against VZV thymidine kinase, the co-crystallized ligand (BVDP-MU) and the three potential lead compounds. The ligand names, PubChem CIDs, plant sources and the intermolecular bonds are included.

Ligand	Pubchem CID	Binding affinity (kcal/mol)	Source Interacting residues Length(Å)	Part of plant	Hydrogen bond length & residues	Hydrophobic interactions
BVDU-MP		−8.9	Co-crystalized ligand		Gly22(3.01); Tyr66(3.22) Gln90(3.05, 3.14); Arg130(2.91);	Tyr21, Glu48, Trp53, Ile62, Phe93, His97, Ala134, Ser135, Phe139,
Acyclovir	135398513	−6.5	Standard drug		Tyr66(3.05,3.93); Gln90(3.08)	Tyr21, Glu48, Trp53, Phe93, Arg130, Ser135, Phe139,
Valacyclovir	135398742	−7.0	Standard drug		Lys25(3.21,3.28); Thr26(2.85) Tyr66(3.24);	Tyr21, Gly22, Gly24, Glu48, Phe93, Arg130, Phe139
Apigenin-4′-Glucoside	5491384	−10.2	*Achillea millefolium*	Leaf and flower head	Gly22(3.23); Gly24(2.88); Gln90(2.70, 3.30)	Tyr21, Ile23, Lys25, Thr26, Glu48, Trp53, Phe93, Arg130, Ala134, Ser135, Phe139
Abyssinone V	6548074	−9.6	*Vitex doniana sweet*	Fruit	Gln90(3.33, 2.70)	Tyr21, Gly22, Lys25, Glu48, Trp53, Ile62, Phe93, Arg130, Ala134, Ser135, Phe139, Val184, Glu192
Myricetin	5281672	−9.3	*Psidium guajava*	Flower	Gly22(3.26), Gln90(2.86)	Tyr21, Glu48, Leu50, Trp53, Phe93, Arg130, Ala134, Ser135, Phe139,

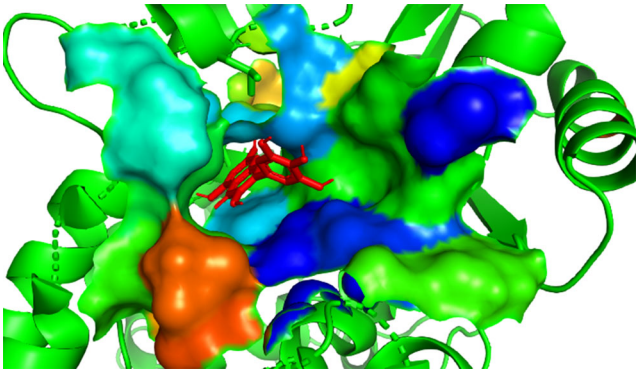

Figure 2. A cartoon representation of the structure of varicella-zoster virus thymidine kinase with abyssinone V (Red stick), myricetin (Cyan blue stick) and apigenin-4′-glucoside (Yellow stick) docked in its binding pocket presented as surface.

3.2. Validation of docking protocol

3.2.1. Alignment and superimposition

Validation of docking protocol is essential in evaluating the efficiency and performance of the AutoDock Vina (Granchi et al., 2015; Heifets & Lilien, 2010). Therefore, the focus of re-docking and superimposition was to validate the docking protocol used. LigAlign (Heifets & Lilien, 2010) script embedded in the PyMol environment was used in validating the protocol. LigAlign uses superimposition of ligands in validating the docking protocol by calculate the Root Mean Square Deviation (RMSD) between the two ligands. This technique is widely adopted for structural analysis of the protein-ligand complex (Heifets & Lilien, 2010). After the redocking, it was observed that these predicted binding poses and the experimentally determined ones shared mutual interactions with specific amino acid residues present within the active site of the protein. When the redocked ligand pose of BVDU-MP of structure 1OSN was superimposed with the co-crystalized ligand (BVDU-MP) (Figure 3a), there were overlaps of hydrogen bonds involving three critical active site residues comprising Arg130, Tyr66 and Gln90 (Figure 3b). In addition, there were overlaps of hydrophobic contacts involving seven residues Ser135, Phe93, Phe139, Ile62, Glu48, Tyr21 and Trp53. These overlaps support the ability of AutoDock Vina to reproduce the experimental binding pose. The RMSD obtained was 0.990 Å (Figure 4), which was within the 2 Å threshold (Alves et al., 2014).

3.2.2. Receiver operating characteristic (ROC) curve

The AutoDock Vina docking protocol used was validated using the ROC curve. The ROC curve is useful when measuring the ability of a docking model to clearly decipher between active compounds from inactive ones with respect to the protein receptor under study (Kwofie, Enninful, et al., 2019). After the ROC curve was generated, the Area Under Curve (AUC) was computed to measure the performance of docking protocol (Mandrekar, 2010). The AUC computed for the study was 0.8099, which is closer to 1, indicating an efficient docking (Mandrekar, 2010). From the results, AutoDock Vina reasonably distinguished active from inactive compounds (Figure 5).

3.3. Characterization of binding mechanism

After the molecular docking studies, the ligands were filtered using the LigPlot^{+} (Laskowski & Swindells, 2011) prediction

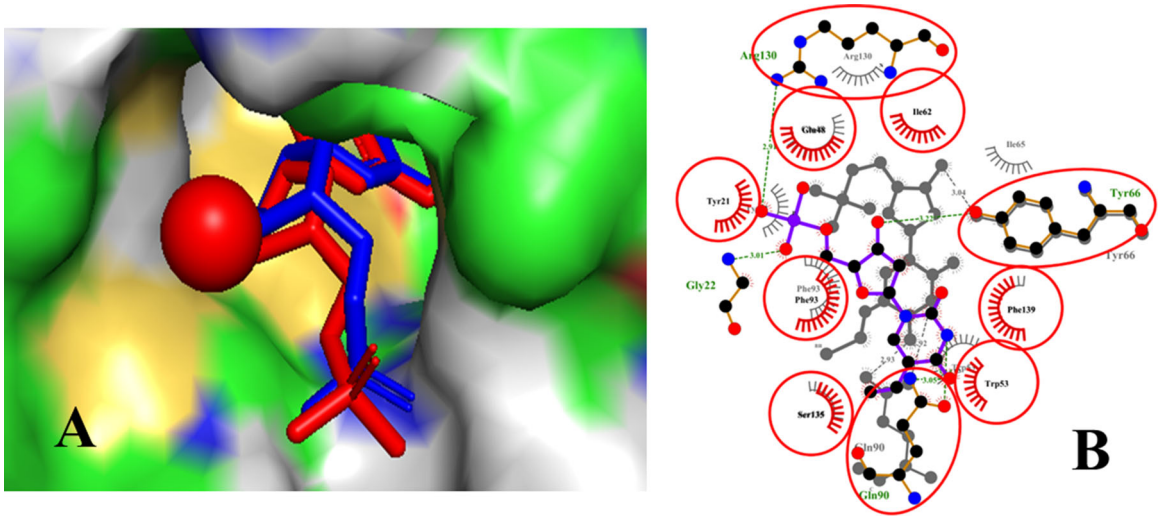

Figure 3. Surface representation of 1OSN with co-crystallized BVDU-MP (red) and re-docked BVDU-MP (blue) its binding pocket (A) and superimposed LigPlot^{+} showing overlapped interactions between the co-crystallized and re-docked ligands (BVDU-MP) (B). The circled residues in red show the overlapped molecular interactions.

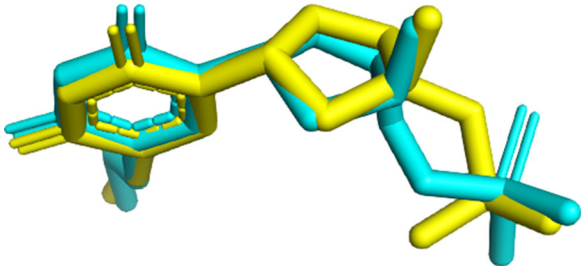

Figure 4. A PyMol representation of the superimposed re-docked BVDU-MP ligand with 1OSN (in cyan blue) and co-crystalized the BVDU-MP ligand of 1OSN with BVDU-MP (in yellow). The RMSD was calculated to be 0.990 Å.

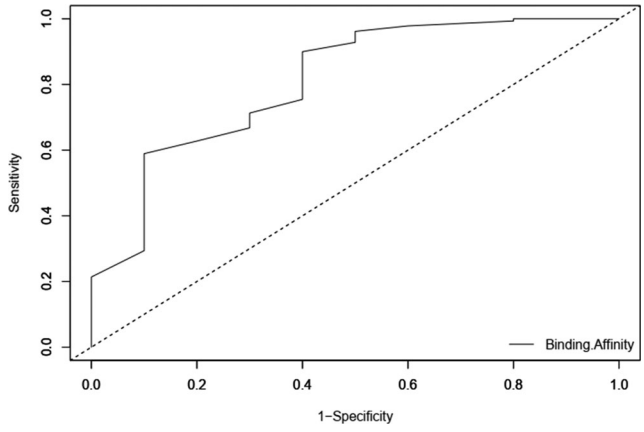

Figure 5. Receiver Operating Characteristic (ROC) curve for varicella-zoster virus thymidine kinase. The curve was obtained after docking 12 actives and 600 decoys against the receptor.

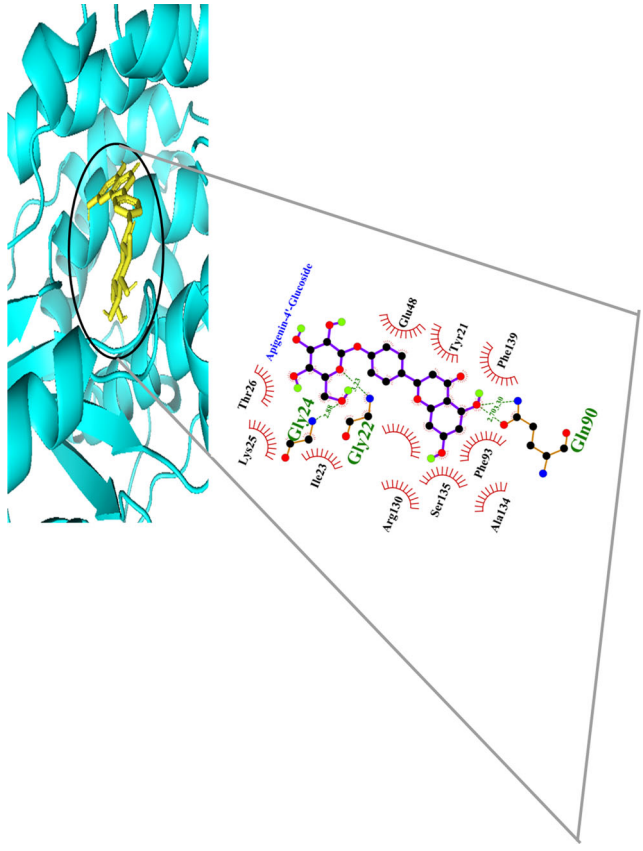

Figure 6. Ligplot^{+} representation of Apigenin-4′-Glucoside in complex with 1OSN showing the intermolecular bonds.

of intermolecular interactions between the ligands and the receptor. Ligands which did not have any interactions with the receptor were excluded from further analysis. Twenty out of the forty-two ligands predicted to have hydrogen bond interactions were used for further analysis (Stilinović et al., 2017) (Supplementary Table 1). For Apigenin-4′-Glucoside, three hydrogen bonds were observed to be formed with the protein target. These bonds were identified to be Gln22, Gly24 and Gln90 with respective bond length of 3.33, 2.88 and 2.79 and 3.38 while hydrophobic interactions were formed between Tyr21, Lys25, Thr26, Glu48, Phe93, Arg130, Ala134, Ser135 and Phe139 (Figure 6). Also, for myricetin, hydrogen bonds were observed to be formed between Gln90 and Gly22 with bond lengths of 2.86 and 3.26 respectively and hydrophobic interactions were formed with Tyr21, Leu50, Trp53, Phe93, Arg130, Ala134 and Phe139 (Supplementary Figure S1). Hydrogen bonds with bond lengths of 3.33 and 2.70 were formed between Abyssinone V

and Gln90 of the protein with hydrophobic interactions involving Tyr21, Gly22, Lys25, Glu48, Trp53, Ile62, Phe93, Arg130, Ala134, Ser135, Phe139, Val184 and Glu192 (Supplementary Figure S2)

3.3. Drug likeness

The drug likeliness of potential lead compounds was evaluated physicochemical parameters. The rules used included the Lipinski rule of five (RO5), the Verber's rule and bioavailability score. According to the Lipinski rule of five, orally active compounds are defined by five parameters which are molecular weight $\leq$ 500 Da, LogP $\leq$ 5, Hydrogen bond donors $\leq$ 5, hydrogen bond acceptors $\leq$ 10, and 40 $\leq$ molar refractivity $\leq$ 140 (Lipinski, 2016). Seven out of the twenty ligands violated the rule, leaving only 13 compounds for further analysis (Table 2). Standard drugs Acyclovir and violated none of the rules (Table 2). The Verber's rule suggests that compounds that meet only the two conditions of ten or fewer rotatable bonds and a polar surface area lesser or equal to 140 $Å^2$ have a high probability of good oral bioavailability (Veber et al., 2002). Results from our study indicated that, out of the 13 ligands that were evaluated with Veber's rule, 10 of them had a polar surface area less than 140 $Å^2$ while three had their polar surface area to be greater than 140 $Å^2$, thus apigenin-4′-glucoside, myricetin and sabine had the polar surface area of 170.05 $Å^2$, 151.59 $Å^2$, 144.85 $Å^2$ respectively (Table 3). Also, valacyclovir, a standard drug had a polar surface area of 151.14 $Å^2$ (Table 3). Bioavailability Score is also used to identify poorly and well absorbed compounds that have been tested in humans (Martin, 2005). Bioavailability Score is expressed as the likelihood that a compound will have >10% bioavailability in rat or quantifiable Caco-2 permeability (Martin, 2005). Bioavailability Score for anions is 0.11, for which TPSA is >150 $Å^2$, 0.56 if TPSA is between 75 and 150 Å2, and 0.85 if PSA is <75$Å^{2,}$ and for the remaining compounds, a bioavailability score is 0.55 for those compounds that obey the Lipinski rule of five and 0.17 for those that violate the law. (Martin, 2005). From our study, a bioavailability score was only assessed on the compounds that conformed to Lipinski rule of 5, and all of them had a bioavailability score of 0.55 (Table 3). This is a confirmation of the compounds' conformity to the rule of 5.

3.4. Prediction of ADME properties

The ADME studies of drug candidates are extensively used in drug discovery to heighten the balance of properties required to convert leads into good drugs (Selick et al., 2002). The three potential leads do not inhibit all three isoforms of the cytochrome P_{450} enzymes, although some of them were observed to inhibit either one or two of the classes (Table 4). Cytochrome P_{450} is an important class of enzyme involved in the metabolism of drugs in the liver (Donato & Castell, 2003). If a drug is predicted to inhibit all the classes of cytochrome P_{450}, it has the potential to impair the metabolism and may lead to toxicity (Donato & Castell, 2003). The blood brain barrier (BBB) is a protective element of the brain that protects the brain from any foreign substance present in the blood. It consists of a barrier that physically separates the blood vessels of the brain from the cells and all the other components of the body (Armulik et al., 2010). It also consist of some enzymes as well as transporters that maintains the integrity of the extracellular environment of the central nervous system (Armulik et al., 2010). In summary, 9 of the ligands that were predicted to have good physiochemical properties were soluble, while 3 were identified to be poorly soluble, and both of the standard drugs were also predicted to be very soluble (Table 4). However, 8 were predicted as BBB impermeant, and 4 were BBB permeant, while both standard drugs were impermeant to the BBB. The four compounds, thus, pinoresinol, achillicin, alpha terpineol and eugenol, that were predicted to be BBB permeant were excluded from further analysis. This is because, compounds that are known to be BBB permeant without having any neurological roles can cause severe effects (Chen & Liu, 2012). Again, 12 compounds were found to be non-inhibitors of the cytochrome P_{450} class of enzymes (Table 4). The 8 compounds that were therefore taken for further analysis are those that were non-inhibitors of the cytochrome P_{450} class of enzymes and also were BBB impermeant.

3.5. Toxicity of ligands

The AMES toxicity, hepatotoxicity, skin sensitization, hERG I inhibitor and the maximum dose of the ligand tolerated in the human body a day were ascertained as a way of predicting the toxicity of these ligands (Pires et al., 2015). Table 5 provides a summary on these properties for each of the compounds. Some of the ligands were predicted to have hepatotoxicity, AMES toxicity, skin sensitization and can be tolerated in the body at average concentrations per day (Table 5). None of the compounds, including the standard drugs was predicted to be an inhibitor of hERG I, a gene that codes for the alpha subunit of the potassium ion channel, best known for how it contributes to the electrical activity of the heart (Hedley et al., 2009). A freely accessible web server, the pKCSM server, which provides an integrated platform to rapidly evaluate pharmacokinetic and toxicity properties was used to assess the toxicity of the ligands. The pKCSM online server uses the graph-based structural signatures concept to study and predict a range of ADMET properties for new chemical entities (Pires et al., 2015). It builds thirty (30) predictors which are divided into five major classes: absorption (seven predictors), distribution (four predictors), metabolism (seven predictors), excretion (two predictors), and toxicity (10 predictors) however, in our study, this server was only used to predict the toxicity of the ligands. The ten (10 toxicity predictors include; AMES toxicity, maximum tolerated dose, oral rat acute toxicity (LD50), oral rat acute toxicity (LOAEL), hepatotoxicity, skin sensitization, T. *Pyriformis* toxicity and minnow toxicity.

3.6. Anti-viral prediction with PASS

The biological activity of the compounds was predicted using the prediction of activity spectra for substances (PASS)

Table 2. Physicochemical properties of active compounds present in *Psidium guajava*, *Vitex doniana sweet* and *Achillea millefolium* using the Lipinski rule of 5. Parameters assessed are molecular weight, number of hydrogen bonds donors, number of hydrogen bond acceptors, logP, and molar refractivity. The number of violations for each compound is also shown.

Ligand	Molecular weight (Dalton)	Number of hydrogen bond donors	Number of hydrogen bond acceptors	$LogP_{o/w}$ (MLOGP)	Molar refractivity	Number of violations
Acyclovir	225	3	5	−1.83	55.68	0
Valacyclovir	324	3	7	−1.19	82.54	0
Campesterin	400	1	1	6.54	128.42	1
Cynaroside	448	7	11	−2.10	108.13	2
Apigenin-4′-Glucoside	432	6	10	−1.61	106.11	1
Luteolin 4′-O-Glucoside	448	7	11	−0.40	105.20	2
Isochlorogenic Acid B	516	7	12	−0.35	126.90	3
Cupreol	414	1	1	6.73	133.23	1
3,5-Dicaffeoylquinic Acid	516	7	12	1.02	125.19	3
Abyssinone V	408	3	5	2.82	119.01	0
Pinoresinol	358	2	6	1.17	94.90	0
Quercetin	302	5	7	1.99	78.03	0
Rutin	610	10	16	−3.89	141.38	4
Achillicin	306	1	5	2.0	80.31	0
Myricetin	318	6	8	−1.08	80.06	1
Guaijaverin	434	7	11	−2.06	104.19	2
Avicularin	434	7	11	−2.06	104.19	2
Achletin	380	3	6	0.05	81.98	0
Sabine	495	7	8	0.60	134.05	1
Alpha terpineol	154	1	1	2.3	48.8	0
Millefin	350	0	6	2.38	92.13	0
Eugenol	164	1	2	2.01	49.06	0

Table 3. Prediction of the oral bioavailability of the ligands using the Veber's rule and bioavailability Score.

Ligand	Topological polar surface area (Å^2)	Number of rotatable bonds	A bioavailability score
Acyclovir	119.05	4	0.55
Valacyclovir	151.14	8	0.55
Campesterin	20.23	5	0.55
Apigenin-4′-Glucoside	170.05	4	0.55
Alpha Elemene	0.00	2	0.55
Cupreol	20.23	6	0.55
Abyssinone V	86.99	5	0.55
Pinoresinol	77.38	4	0.55
Quercetin	131.36	1	0.55
Achillicin	72.83	2	0.55
Myricetin	151.59	1	0.55
Achletin	135.12	2	0.55
Sabine	144.85	0	0.55
Alpha terpineol	20.23	1	0.55
Millefin	78.90	4	0.55
Eugenol	29.46	3	0.55

Table 4. Prediction of adsorption, distribution, metabolism and excretion (ADME) properties of selected ligands. Water solubility of the ligands, class of solubility, BBB permeability, gastrointestinal absorption, Cytochrome P_{450} inhibition and P-glycoprotein substrate were computed.

Ligand	Water solubility; LogS (ESOL)	Class of solubility	BBB permeability	Gastrointestinal absorption	CYP1A2 inhibition	CYP2C19 inhibition	CYP3A4 inhibition	P-Glycoprotein substrate
Acyclovir	−0.41	Very soluble	No	High	No	No	No	No
Valacyclovir	−1.23	Very soluble	No	Low	No	No	No	Yes
Campesterin	−7.54	Poorly soluble	No	Low	No	No	No	No
Apigenin-4′-Glucoside	−3.41	Soluble	No	Low	No	No	No	Yes
Cupreol	−7.90	Poorly soluble	No	Low	No	No	No	No
Abyssinone V	−6.35	Poorly soluble	No	High	No	No	Yes	No
Pinoresinol	−3.58	Soluble	Yes	High	No	No	Yes	Yes
Quercetin	−3.16	Soluble	No	High	Yes	No	Yes	No
Achillicin	−1.97	Very soluble	Yes	High	No	No	No	No
Myricetin	−3.01	Soluble	No	Low	Yes	No	Yes	No
Achletin	−2.64	Soluble	No	High	No	No	No	No
Alpha terpineol	−2.87	Soluble	Yes	High	No	No	No	No
Millefin	−3.01	Soluble	No	High	No	No	No	No
Eugenol	−2.46	Soluble	Yes	High	Yes	No	No	No

Table 5. Prediction of the toxicity of the selected ligands. The AMES toxicity, hepatotoxicity, the maximum tolerated dose per day of the ligand, skin sensitization and hERG 1 inhibition were ascertained using pKCSM.

Ligand	AMES toxicity	Hepatotoxicity	Max. tolerated dose (mg/kg/day)	Skin sensitization	hERG I inhibitor
Acyclovir	Yes	Yes	2.655	No	No
Valacyclovir	No	Yes	3.556	No	No
Apigenin-4′-Glucoside	No	No	2.938	No	No
Campesterol	No	No	0.348	No	No
Cupreol	No	No	0.239	No	No
Abyssinone V	No	No	1.706	No	No
Quercetin	No	No	3.155	No	No
Myricetin	No	No	3.235	No	No
Achletin	Yes	Yes	2.254	No	No
Millefin	No	No	2.213	No	No

online server, which provides the probability of activity (Pa) and the probability of inactivity (Pi). The PASS online software product contains 31,000 biologically active substances in the training set and predicts biological activity for 319 types of pharmacological effects, biological mechanism of actions as well as specific toxicity of the substances with an average accuracy above 95%(Lagunin et al., 2000). Biological activities with $P_a > P_i$ are considered as worthy of pharmacological evaluation (Goel et al., 2011). Our study considered the antiviral herpes activity of the molecules since the varicella-zoster virus belong to the family *Herpesviridae* (Camacho-Soto et al., 2021; Wang et al., 2020). Out of 9 compounds shortlisted, only 3 of them namely myricetin, apigenin-4′-glucoside and Abyssinone V were predicted as having anti-herpes activity with Pa $\geq$ 0.5 (Table 6). However, the known drugs were predicted to have Pa $>$ 0.7. The two- and three-dimensional structures of the potential leads are shown in Table 7.

3.7. Binding mechanisms of the potential lead compounds

The potential lead compounds identified were myricetin from the fruit *Psidium guajava*, apigenin-4′-glucoside from the leaf of *Achillea millefolium*, and Abyssinone V from the fruit *Vitex doniana Sweet*. Apigenin-4′- glucoside exhibited binding affinity of −10.2 kcal/mol against the receptor by forming four hydrogen bond interactions (Table 1) with active site residues Gly24, Gly22 and Gln90, and hydrophobic contacts Lys25, Thr26, Glu48, Tyr21, Phe139, Phe93, Ser135, Arg130, Trp53, Ile23 and Ala134. This was followed by Abyssinone V with binding affinity of −9.6 kcal/mol forming two hydrogen bond interactions with Gln90 and hydrophobic contacts with Ser135, Ala134, Phe93, Trp53, Arg130, Gly22, Lys25, Phe139, Ile62, Glu192, Val184, Tyr21 and Glu48 (Table 1). Finally, myricetin also had a binding affinity of −9.3 kcal/mol and formed two hydrogen bonds with key residues Gly22 and Gln90, while interacting via hydrophobic interactions with Leu50, Glu48, Tyr21, Trp53, Ala134, Ser135, Phe93, Phe139 and Arg130. From our study, Ala134 is also predicted as likely to be a novel critical residue involved in the activity of the protein since it formed intermolecular bonds with all the potential lead compounds, as well as the known drugs and the co-crystallized BVDU-MP.

3.8. Molecular dynamic simulations and MM-PBSA

MD simulation was carried out for the ligand-protein complexes and the Root Mean Square Deviation (RMSD), Root Mean Square Fluctuation (RMSF) and radius of gyration (Rg) (Peele et al., 2020) were computed for each of the three potential leads together with the co-crystalized ligand (BVDU-MP) and the known drug acyclovir (Figures 7–9). MD simulations predicted how these potential lead compounds forms stable complexes with the target protein (Al-Khafaji et al., 2020). The RMSD computed for all complexes indicates stability of the protein even after docking (Al-Khafaji et al., 2020). For the co-crystallized ligand BVDU-MP, the RMSD curve predicts a very high stability as the curve plateaued at 0.2 nm from 0.5 ns of MD run (Figure 7) till the 100 ns run was done. The three potential lead-complexes showed great stability with RMSD values ranging from 0.3 nm to 0.7 nm, mostly peaking after 20 ns. The most stable among the three however was apigenin-4′-glucoside-complex with RMSD of 0.3 nm, followed by myricetin with 0.5 nm, and then abyssinone V with 0.7 nm (Figure 7). The RMSF values indicates flexibility in different regions of the protein (Islam et al., 2021). For the co-crystallized ligand BVDU-MP, the highest fluctuation occurred in the region between atoms 600 and 700 (Figure 8), after which there was great stability till the end of the run. Also, highest fluctuations were observed between atoms 500 and 1000, 1600 and 2000 for abyssinone V and myricetin, respectively (Figure 8). Apigenin- 4′- glucoside showed fairly little fluctuations along such regions. Greater amounts of structural fluctuation occur in regions known to be involved in ligand binding and catalysis (Dong et al., 2018). RMSF of abyssinone V showed exceptionally much greater fluctuations at these atomic regions which depicts greater adaptive variations in flexibility which can increase the conformational stability of abyssinone V as compared to the other lead compounds in the protein complex. The radius of gyration values indicates the compactness of the complex structures (Islam et al., 2021). Rg values ranged from 1.85 nm to 1.95 nm for the complexes of potential leads and the known inhibitors (Figure 9), respectively, which were similar to those reported previously (Kwofie et al., 2021).

3.8.1. Per-residue energy decomposition of VZV thymidine kinase-ligand complexes

MM-PBSA was carried out on the complexes of the three potential leads and two known inhibitors. Per-residue energy decomposition of VZV TK-ligand enables the calculation of

Table 6. Prediction of the biological activities of potential lead compounds using PASS determined with Probable activity (Pa) and Probable inactivity (Pi).

Ligand	Activity	Probable activity (P_a)	Probable inactivity (P_i)
	Antiviral	0.309	0.033
	Antiviral (Hepatitis B)	0.490	0.005
	Antiviral (Herpes)	0.552	0.006
Apigenin-4′-Glucoside	Antiviral (Influenza)	0.730	0.004
	Antiviral (Picornavirus)	0.301	0.226
	DNA ligase (ATP) inhibitor	0.656	0.002
	DNA polymerase I inhibitor	0.395	0.021
	DNA repair enzyme inhibitor	0.319	0.004
	DNA synthesis inhibitor	0.502	0.018
	Antiviral (Hepatitis B)	0.384	0.017
Abyssinone V	Antiviral (Herpes)	0.504	0.009
	Antiviral (Influenza)	0.575	0.015
	Antiviral (Rhinovirus)	0.590	0.007
	DNA ligase (ATP) inhibitor	0.328	0.035
	Antiviral	0.334	0.026
Myricetin	Antiviral (Hepatitis B)	0.519	0.004
	Antiviral (Herpes)	0.500	0.010
	Antiviral (Influenza)	0.444	0.034
	DNA ligase (ATP) inhibitor	0.564	0.004

Table 7. Ligand names, PubChem CIB, 2-Dimensional and 3-Dimensional structures of potential lead compounds predicted.

Ligand	Pubchem CID	2_Dimensional structure	3_Dimensional sturcture
Myrecitin	5281672	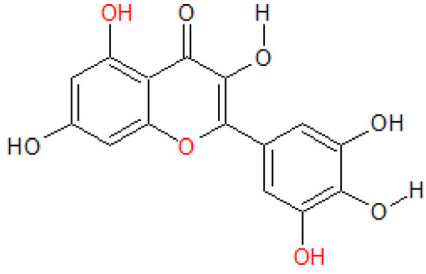	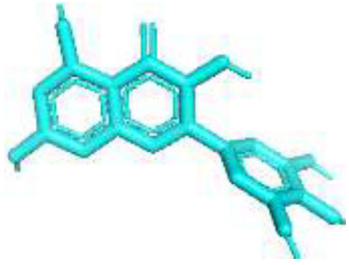
Apigenin-4′-Glucoside	5491384	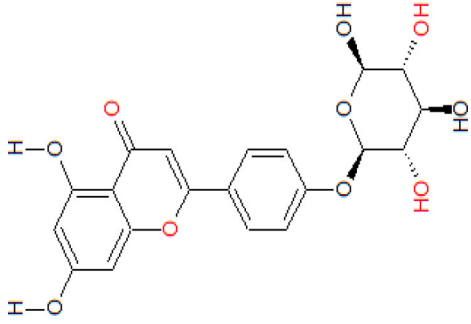	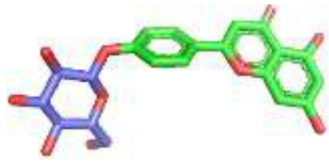
Abyssinone V	6548074	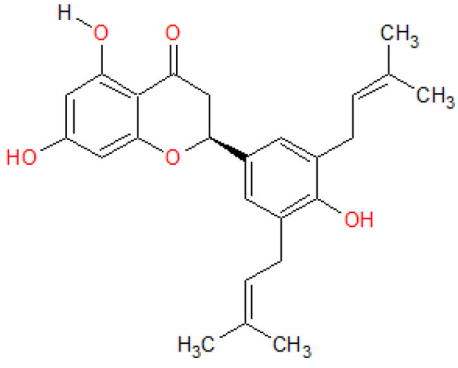	

energy contribution for each residue. Residues contributing binding free energy greater than 5 kJ/mol or less than −5 kJ/mol are considered as critical for binding of a ligand to a protein (Kwofie, Dankwa, et al., 2019). For the VZV TK-myricetin complex, hydrophobic residues Tyr21 (−7.5619 kJ/mol) and Glu48(8.4539 kJ/mol) were immensely involved in contributing to the free binding energy of the complex (Figure 10). Hydrogen bond forming residues Gly22 (−0.7751) and Gln90 (−0.1436) did not contribute significantly. For the complex VZV-TK-abyssinone V, the critical active site residues that

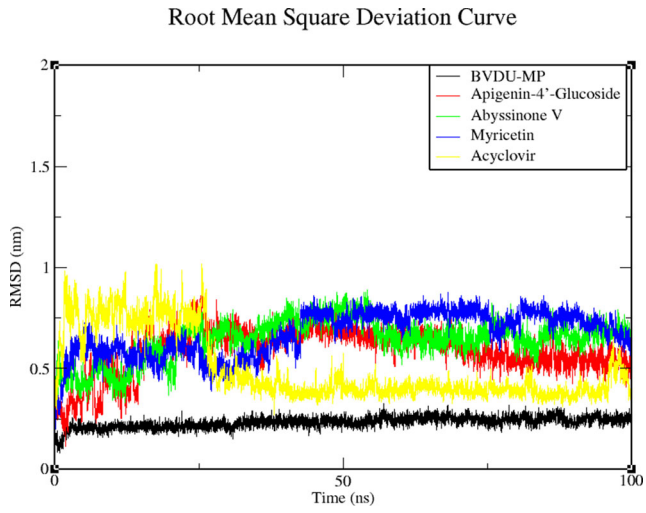

Figure 7. RMSD trajectories of the complexes calculated for the 100 ns simulation timescale. Graphs are represented in different colors with black, red, green, blue and yellow legend representing BVDU-MP, apigenin-4′-glucoside, abyssinone V, myricetin and known drug (acyclovir), respectively.

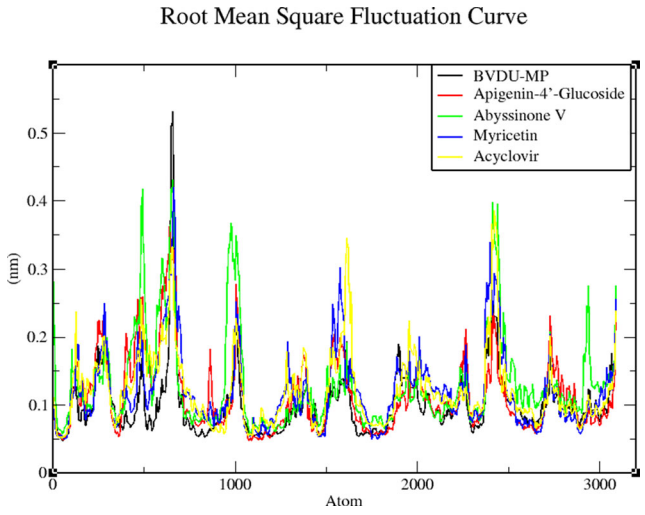

Figure 8. RMSF trajectories of the complexes computed for 100 ns simulation timescale. Graphs are represented in different colors with black, red, green, blue and yellow legend representing BVDU-MP, apigenin-4′-glucoside, abyssinone V, myricetin and known drug (acyclovir), respectively.

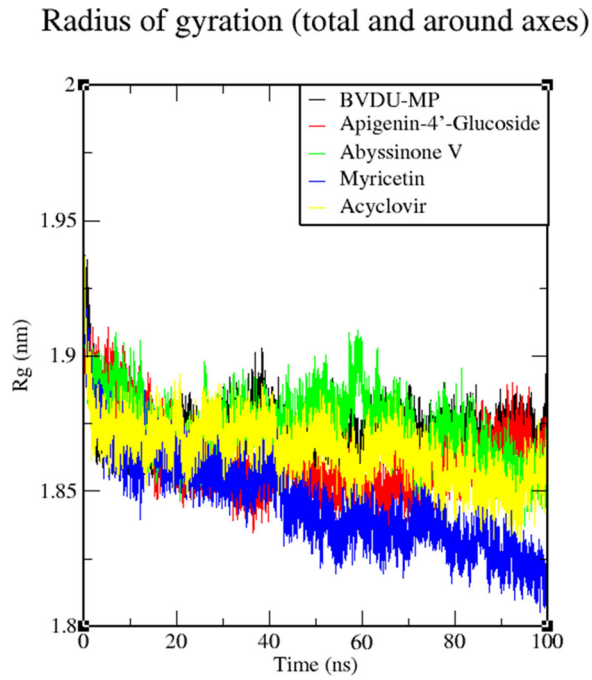

Figure 9. Radius of Gyration trajectories of the complexes computed for the 100 ns simulation timescale. Graphs are represented in different colors with black, red, green, blue and yellow legend representing BVDU-MP, apigenin-4′-glucoside, abyssinone V, myricetin and known drug (acyclovir), respectively.

contributed to the free binding energy was observed to be Trp53 (−12.7773 kJ/mol), Phe93 (−14.973 kJ/mol) and Ser135 (7.7566 kJ/mol), all of which formed hydrophobic interaction with the ligand. (Supplementary Figure S1). For the complex VZV TK-apigenin-4′-glucoside, Tyr21 (−10.1107 kJ/mol), Trp53 (−7.6053 kJ/mol), Phe93 (−12.7869 kJ/mol), Ser135 (−9.7755 kJ/mol), could be considered as the critical residues that contributed immensely towards the binding energy of the complex (Supplementary Figure S2). For acyclovir-VZV TK complex, residues Tyr21 (−6.7216 kJ/mol), Glu48 (7.5788 kJ/mol) and Tyr66 (−5.772 kJ/mol) were observed to interact with the ligand from the docking analysis was corroborated after MM-PBSA (Supplementary Figure S3). For the co-crystallized ligand BVDU-MP in complex with VZV-TK, Tyr21 (−10.9787 kJ/mol) and Glu48 (101.4915 kJ/mol) Tyr66 (−8.9697 kJ/mol) Phe93 (−13.3358 kJ/mol) Ser135 (−55.7476 kJ/mol) contributed significant energies (Supplementary Figure S4). The residues Gly22 and Tyr66 formed hydrogen bonds with those which also formed hydrophobic contacts. Identified critical active site residues contributing significant free binding energy included Try21, Gly22, Glu48, Trp53, Tyr66, Phe93 and Ser135.

3.8.2. Other energy terms

Van der Waals forces, electrostatic and polar solvation energies were useful in estimating the free binding energy of the complex. The van der Waals refers to the weak attraction existing between the intermolecular forces (Geesink & Meijer, 2021). The van der Waals energy observed in our study ranged between −165.737 kJ/mol and −256.232 kJ/mol with apigenin-4′-glucoside having the least van der Waals energy of −256.232 kJ/mol among the potential lead molecules, while myricetin exhibited the highest energy of −165.737 kJ/mol (Table 8). Meanwhile, abyssinone V had van der Waals energy of −206.928 kJ/mol. Among the known inhibitors, BVDU-MP and acyclovir close der Waals energy of −134.824 kJ/mol and −135.341 kJ/mol, respectively.

Electrostatic energy refers to the potential energy of a system consisting of different electric charges (Tort, 2013). Electrostatic energy was observed between −41.863 kJ/mol and −305.504 kJ/mol (Table 8). Among the potential lead compounds, myricetin showed the least electrostatic energy of −84.341 kJ/mol, followed by apigenin-4′-glucoside with −58.034 kJ/mol, and then abyssinone with −52.967 kJ/mol. For the known inhibitors, BVDU-MP had the least electrostatic energy of −305.504 kJ/mol whilst acyclovir had −41.863 kJ/mol. Polar solvation energy also represents the electrostatic interaction that exists between the solute and the continuum solvent (Genheden & Ryde, 2015). The polar solvation energy was between 113.934 kJ/mol and

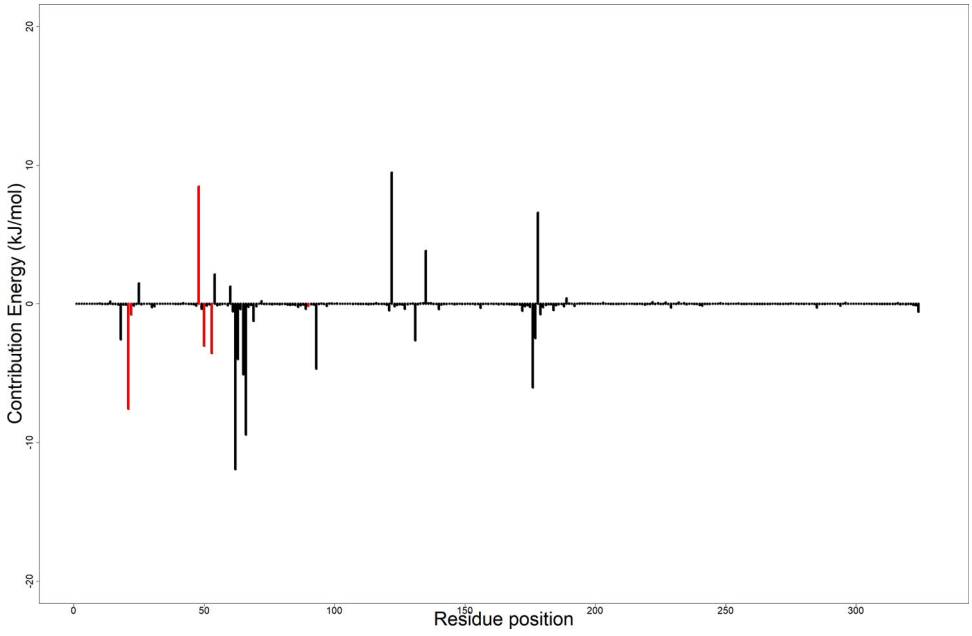

Figure 10. MM-PBSA plot of the binding free energy decomposition contribution per residue of VZV thymidine kinase-myricetin complex. Coded red lines represent surrounding active site amino acid residues.

Table 8. Energy component terms of the VZV thymidine kinase-ligand complexes calculated using MM-PBSA. The values are reported in average ± standard deviation in kJ/mol.

Compounds	van der Waals energy (kJ/mol)	Electrostatic energy (kJ/mol)	Polar solvation energy (kJ/mol)	Solvent accessible surface area (SASA) energy (kJ/mol)	Binding energy (kJ/mol)
Myricetin	−165.737 ± 16.432	−84.341 ± 20.423	160.018 ± 24.013	−14.445 ± 0.901	−104.505 ± 24.308
Apigenin-4′-Glucoside	−256.232 ± 23.993	−58.034 ± 25.530	163.804 ± 35.412	−20.080 ± 1.309	−170.543 ± 28.435
Abyssinone V	−206.928 ± 17.607	−52.967 ± 20.513	150.983 ± 25.246	−18.762 ± 1.224	−127.673 ± 21.786
Acyclovir	−135.341 ± 13.993	−41.863 ± 18.458	113.934 ± 32.252	−13.152 ± 1.004	−76.422 ± 22.551
BVDU-MP	−134.824 ± 18.030	−305.504 ± 77.852	838.082 ± 59.272	−16.905 ± 0.724	380.850 ± 38.693

838.082 kJ/mol, and acyclovir had the least polar solvation energy of 113.934 kJ/mol. Abyssinone V, myricetin, apigenin-4′-glucoside and BVDU-MP had polar solvation energies of 150.983, 160.018, 163.804 and 838.082 kJ/mol, respectively.

Furthermore, Solvent Accessible Surface Area (SASA) energy represents the non-polar solvation energy (Genheden & Ryde, 2015). This energy measures the interactions that exist between the complex and the solvents. The SASA energies obtained were −13.152 kJ/mol, −14.445 kJ/mol, −16.905 kJ/mol, −18.762 kJ/mol and −20.080 kJ/mol for acyclovir, myricetin, BVDU-MP, abyssinone V and apigenin-4′-glucoside, respectively (Table 8).

Acyclovir demonstrated the highest binding affinity with a binding free energy of −76.422 kJ/mol. This was followed by myricetin, abyssinone V, apigenin-4′-glucoside, and BVDU-MP with binding free energies of −104.505, −127.673, −170.54 and 380.850 kJ/mol, respectively (Table 8). The low binding free energies exhibited by these compounds demonstrate their propensity to be potential inhibitory molecules of VZV TK worthy of *in vitro and in vivo* studies.

3.9. Exploring known mechanism of action and biological activity of predicted leads

All three molecules identified in our study have been reported to have antiviral activities (Grienke et al., 2016; Khan et al., 2020; Sang et al., 2021). This corroborate the predictions made with PASS in the earlier addressed PASS results. Myricetin has been investigated act to reduce ATPase activity by inhibiting the nonstructural protein 13 (nsp13) of coronaviruses (Yu et al., 2012). Also, it has been investigated *in vitro* to have potential activity against the *Herpesviridae* family of viruses (Li et al., 2020), of which the varicella-zoster virus is a member. It has the ability to block the *Herpes Simplex* Virus (HSV) I and II by directly interacting with the glycoprotein D (gD), a structural component of this family of viruses (Li et al., 2020). This activity interferes in the absorption as well as the membrane fusion of the virus, thereby inhibiting its replication (Li et al., 2020). Further investigations *in vitro* can therefore be carried out to corroborate the predicted ability of myricetin to inhibit the activity of the varicella-zoster virus. Apigenin, a derivative of Apigenin-4′-Glucoside is a constituent in the genus *Nepeta*, and these plants have been extensively used for treating chicken pox (Sharma et al., 2021). By increasing the membrane permeability of protein, disrupting and depolarizing cell membrane integrity, reducing the activity of enzymes bound to membrane as well as inducing apoptosis, this genus of plants are able to exhibit cytotoxic effects, thereby impairing viral growth and subsequent replication (Sharma et al., 2021). Abyssinone V, has also been reported to inhibit pneumococcal neuraminidase (NA), a critical target for influenza with

IC_{50} = 2.18 μM, and pneumococcal growth with MIC = 5.63 μM, without causing any disadvantage to the lung epithelial cells (Grienke et al., 2016). It is therefore imperative and worth investigating these potential therapeutic molecules, since they can be of great relevance to the treatment of the chicken pox infection.

4. Conclusion

The study identified 3 potential lead compounds comprising myricetin, apigenin-4′-glucoside and abyssinone V out of a total of 65 obtained from three different plants used traditionally as treatment for chicken pox. The study docked the molecules against the X-ray structure of VZV thymidine kinase and used MD simulations including MM-PBSA to gain novel insights into the binding mechanisms. The compounds were predicted as possessing antiviral activity including antiherpes and inhibitors of polymerase, ATPase and membrane integrity. Previous *in vitro* studies corroborated the biological activities in other viruses. In addition, apigenin derivative is a constituent of plant genus used as crude extract treatment for chicken pox. The molecules were shown to have good pharmacological profiles with insignificant toxicity. Therefore, it is essential to experimentally determine their activity *in vitro* to support the predicted activity against VZV thymidine kinase. These molecules could be useful in the designing of novel scaffolds for future therapeutic agents for chicken pox.

Acknowledgements

The authors of this research are grateful to the West African Centre for Cell Biology of Infectious Pathogens (WACCBIP) at the University of Ghana for making Zuputo, a Dell EMC high-performance computing cluster, available for this study

Disclosure statement

No potential conflict of interest was reported by the authors.

ORCID

Samuel Kojo Kwofie http://orcid.org/0000-0002-1093-1517
Cynthia Ayefoumi Adinortey http://orcid.org/0000-0001-8569-8433
Daniel Boison http://orcid.org/0000-0002-2242-7502
Michael Buenor Adinortey http://orcid.org/0000-0001-8287-7460

Author contributions

MBA and SKK conceptualized the research project. DGA MBA, SKK, CAA, DB, GBK and RAA carried out different aspects of computational analysis. Data analysis and interpretation was done by DGA MBA, SKK, CAA, DB, GBK and RAA. MBA, DGA and SKK wrote the first draft. Revision of draft was done by DGA MBA, SKK, CAA, DB, GBK and RAA. Approval of final manuscript was done by DGA, MBA, SKK, CAA, DB, RAA and GBK.

Data availability statement

All data and their identifications (IDs) used in this work are available in the manuscript and the supplementary paper.

References

Abo Almaali, H. (2018). Molecular docking of some peptides to varicella zoster virus drug targets. *Albahir Journal*, *7*, 13–14.
Ajiboye, T. (2015). Standardized extract of Vitex doniana Sweet stalls protein oxidation, lipid peroxidation and DNA fragmention in acetaminophen-induced hepatotoxicity. *Journal of Ethnopharmacology*, *164*, 273–282. https://doi.org/10.1016/j.jep.2015.01.026
Al-Khafaji, K., Al-Duhaidahawi, D., & Taskin Tok, T. (2020). Using integrated computational approaches to identify safe and rapid treatment for SARS-CoV-2. *Journal of Biomolecular Structure and Dynamics*, *39*(9), 1–9. https://doi.org/10.1080/07391102.2020.1764392
Alves, M. J., Froufe, H. J. C., Costa, A. F. T., Santos, A. F., Oliveira, L. G., Osório, S. R. M., Abreu, R. M. V., Pintado, M., & Ferreira, I. C. F. R. (2014). Docking studies in target proteins involved in antibacterial action mechanisms: Extending the knowledge on standard antibiotics to antimicrobial mushroom compounds. *Molecules (Basel, Switzerland)*, *19*(2), 1672–1684. Multidisciplinary Digital Publishing Institute), https://doi.org/10.3390/molecules19021672
Andrei, G., & Snoeck, R. (2011). Engineering drugs for varicella-zoster virus infections. *Expert Opinion on Emerging Drugs*, *16*(3), 507–535. https://doi.org/10.1517/14728214.2011.591786
Angamuthu, D., Purushothaman, I., Kothandan, S., & Swaminathan, R. (2019). Antiviral study on Punica granatum L., Momordica charantia L., Andrographis paniculata Nees, and Melia azedarach L., to Human Herpes Virus-3. *European Journal of Integrative Medicine*, *28*, 98–108. https://doi.org/10.1016/j.eujim.2019.04.008
Applequist, W. L., & Moerman, D. E. (2011). Yarrow (Achillea millefolium L.): A neglected panacea? A review of ethnobotany, bioactivity, and biomedical research. *Economic Botany*, *65*(2), 209–225. https://doi.org/10.1007/s12231-011-9154-3
Armulik, A., Genové, G., Mäe, M., Nisancioglu, M. H., Wallgard, E., Niaudet, C., He, L., Norlin, J., Lindblom, P., Strittmatter, K., Johansson, B. R., & Betsholtz, C. (2010). Pericytes regulate the blood–brain barrier. *Nature*, *468*(7323), 557–561.
Artemova, S., Jaillet, L., & Redon, S. (2016). Automatic molecular structure perception for the universal force field. *Journal of Computational Chemistry*, *37*(13), 1191–1205.
Arvin, A. M. (1996). Varicella-zoster virus. *Clinical Microbiology Reviews*, *9*(3), 361–381. https://doi.org/10.1128/CMR.9.3.361
Ayitey-Smith, E. (1989). *Prospects and scope of plant medicine in health care*. University of Ghana.
Balfour, H. H., Jr., Edelman, C. K., Anderson, R. S., Reed, N. V., Slivken, R. M., Marmor, L. H., Dix, L., Aeppli, D., & Talarico, C. L. (2001). Controlled trial of acyclovir for chickenpox evaluating time of initiation and duration of therapy and viral resistance. *The Pediatric Infectious Disease Journal*, *20*(10), 919–926. https://doi.org/10.1097/00006454-200110000-00002
Baxter, R., Ray, P., Tran, T. N., Black, S., Shinefield, H. R., Coplan, P. M., Lewis, E., Fireman, B., & Saddier, P. (2013). Long- term effectiveness of caricella vaccine: A 14-year, prospective cohort study. *PEDIATRICS*, *131*(5), e1389–e1396. https://doi.org/10.1542/peds.2012-3303
Benedek, B., & Kopp, B. (2007). Achillea millefolium L. sl revisited: Recent findings confirm the traditional use. *Wiener Medizinische Wochenschrift*, *157*(13–14), 312–314. https://doi.org/10.1007/s10354-007-0431-9
Bird, L. E., Ren, J., Wright, A., Leslie, K. D., Degrève, B., Balzarini, J., & Stammers, D. K. (2003). Crystal structure of varicella zoster virus thymidine kinase. *Journal of Biological Chemistry*, *278*(27), 24680–24687. https://doi.org/10.1074/jbc.M302025200
Bonsu, A. (2012). *Healing with simple plants*. Radiant Health Publications.
Camacho-Soto, A., Faust, I., Racette, B. A., Clifford, D. B., Checkoway, H., & Nielsen, S. S. (2021). Herpesvirus infections and risk of Parkinson's disease. *Neurodegenerative Diseases*, *20*(2-3), 97–103.
Chandler, R. F., Hooper, S. N., & Harvey, M. J. (1982). Ethnobotany and phytochemistry of yarrow, Achillea millefolium, Compositae. *Economic Botany*, *36*(2), 203–223. https://doi.org/10.1007/BF02858720
Chen, Y., & Liu, L. (2012). Modern methods for delivery of drugs across the blood-brain barrier. *Advanced Drug Delivery Reviews*, *64*(7), 640–665. https://doi.org/10.1016/j.addr.2011.11.010

Chou, S., & Lurain, N. S. (2019). Antiviral consideration for transplantation including drug resistance. In Safdar Amar (Ed.), *Principles and practice of transplant infectious diseases* (pp. 953–975). New York, NY: Springer.

Civen, R., Chaves, S. S., Jumaan, A., Wu, H., Mascola, L., Gargiullo, P., & Seward, J. F. (2009). The incidence and clinical characteristics of herpes zoster among children and adolescents after implementation of varicella vaccination. *Pediatric Infectious Disease Journal*, *28*(11), 954–959. https://doi.org/10.1097/INF.0b013e3181a90b16

Cohen, J. I., Brunell, P. A., Straus, S. E., & Krause, P. R. (1999). Recent advances in varicella-zoster virus infection. *Annals of Internal Medicine*, *130*(11), 922–932.

Daina, A., Michielin, O., & Zoete, V. (2017). SwissADME: A free web tool to evaluate pharmacokinetics, drug-likeness and medicinal chemistry friendliness of small molecules. *Scientific Reports*, *7*(1), 42717–42713. https://doi.org/10.1038/srep42717

Dallakyan, S., & Olson, A. J. (2015). Small-molecule library screening by docking with PyRx. *Methods in Molecular Biology (Clifton, N.J.)*, *1263*, 243–250. https://doi.org/10.1007/978-1-4939-2269-7_19

Donato, M. T., & Castell, J. V. (2003). Strategies and molecular probes to investigate the role of cytochrome P450 in drug metabolism. *Clinical Pharmacokinetics*, *42*(2), 153–178.

Dong, Y-w., Liao, M-l., Meng, X-l., & Somero, G. N. (2018). Structural flexibility and protein adaptation to temperature: Molecular dynamics analysis of malate dehydrogenases of marine molluscs. *Proceedings of the National Academy of Sciences*, *115*(6), 1274–1279. https://doi.org/10.1073/pnas.1718910115

Essmann, U., Perera, L., Berkowitz, M. L., Darden, T., Lee, H., & Pedersen, L. G. (1995). A smooth particle mesh Ewald method. *The Journal of Chemical Physics*, *103*(19), 8577–8593. https://doi.org/10.1063/1.470117

Eyog Matig, O., Gaoué, O., & Dossou, B. (éditeurs). (2002). *Réseau «Espèces Ligneuses Alimentaires». Compte rendu de la première réunion du Réseau tenue 11–13 décembre 2000 au CNSF Ouagadougou, Burkina Faso*. Institut International des Ressources Phytogénétiques.

Filimonov, D., Lagunin, A., Gloriozova, T., Rudik, A., Druzhilovskii, D., Pogodin, P., & Poroikov, V. (2014). Prediction of the biological activity spectra of organic compounds using the PASS online web resource. *Chemistry of Heterocyclic Compounds*, *50*(3), 444–457. https://doi.org/10.1007/s10593-014-1496-1

Floret, D. (2005). Immunization against varicella. *Therapie*, *60*(3), 275–282. https://doi.org/10.2515/therapie:2005036

Geesink, H. J., & Meijer, D. K. (2021). A predictive model that reveals a causal relation between exposures to non-thermal electromagnetic waves and biological effects (update January 2021).

Genheden, S., & Ryde, U. (2015). The MM/PBSA and MM/GBSA methods to estimate ligand-binding affinities. *Expert Opinion on Drug Discovery*, *10*(5), 449–461. https://doi.org/10.1517/17460441.2015.1032936

Gershon, A. A. (2017). Is chickenpox so bad, what do we know about immunity to varicella zoster virus, and what does it tell us about the future? *Journal of Infection*, *74*, S27–S33. https://doi.org/10.1016/S0163-4453(17)30188-3

Goel, R. K., Singh, D., Lagunin, A., & Poroikov, V. (2011). PASS-assisted exploration of new therapeutic potential of natural products. *Medicinal Chemistry Research*, *20*(9), 1509–2523. https://doi.org/10.1007/s00044-010-9398-y

Goksuluk, D., Korkmaz, S., Zararsiz, G., & Karaagaoglu, A. E. (2016). easyROC: An interactive web-tool for ROC curve analysis using R language environment. *The R Journal*, *8*(2), 213. https://doi.org/10.32614/RJ-2016-042

Granchi, C., Capecchi, A., Del Frate, G., Martinelli, A., Macchia, M., Minutolo, F., & Tuccinardi, T. (2015). Development and validation of a docking-based virtual screening platform for the identification of new lactate dehydrogenase inhibitors. *Molecules (Basel, Switzerland)*, *20*(5), 8772–8790.

Grienke, U., Richter, M., Walther, E., Hoffmann, A., Kirchmair, J., Makarov, V., Nietzsche, S., Schmidtke, M., & Rollinger, J. M. (2016). Discovery of prenylated flavonoids with dual activity against influenza virus and Streptococcus pneumoniae. *Scientific Reports*, *6*(1), 27156–27111. https://doi.org/10.1038/srep27156

Guex, N., Peitsch, M. C., & Schwede, T. (2009). Automated comparative protein structure modeling with SWISS-MODEL and Swiss-PdbViewer: a historical perspective. *Electrophoresis*, *30*(S1), S162–S173. https://doi.org/10.1002/elps.200900140

Gutierrez, R. M., Mitchell, S., & Solis, R. V. (2008). Psidium guajava: A review of its traditional uses, phytochemistry and pharmacology. *Journal of Ethnopharmacology*, *117*(1), 1–27. https://doi.org/10.1016/j.jep.2008.01.025

Hedley, P. L., Jørgensen, P., Schlamowitz, S., Wangari, R., Moolman-Smook, J., Brink, P. A., Kanters, J. K., Corfield, V. A., & Christiansen, M. (2009). The genetic basis of long QT and short QT syndromes: A mutation update. *Human Mutation*, *30*(11), 1486–1511. https://doi.org/10.1002/humu.21106

Heifets, A., & Lilien, R. H. (2010). LigAlign: Flexible ligand-based active site alignment and analysis. *Journal of Molecular Graphics & Modelling*, *29*(1), 93–101. https://doi.org/10.1016/j.jmgm.2010.05.005

Heininger, U., & Seward, J. F. (2006). Varicella. *The Lancet*, *368*(9544), 1365–1376. https://doi.org/10.1016/S0140-6736(06)69561-5

Hoffmann, A., Doring, K., Seeger, N. T., Buhler, M., Schacke, M., Krumbholz, A., & Sauerbrei, A. (2017). Genetic polymorphism of thymidine kinase (TK) and DNA polymerase (pol) of clinical varicella-zoster virus (VZV) isolates collected over three decades. *Journal of Clinical Virology : The Official Publication of the Pan American Society for Clinical Virology*, *95*, 61–65. https://doi.org/10.1016/j.jcv.2017.08.011

Huie, C. W. (2002). A review of modern sample-preparation techniques for the extraction and analysis of medicinal plants. *Analytical and Bioanalytical Chemistry*, *373*(1–2), 23–30. https://doi.org/10.1007/s00216-002-1265-3

Islam, R., Parves, M. R., Paul, A. S., Uddin, N., Rahman, M. S., Mamun, A. A., Hossain, M. N., Ali, M. A., & Halim, M. A. (2021). A molecular modeling approach to identify effective antiviral phytochemicals against the main protease of SARS-CoV-2. *Journal of Biomolecular Structure & Dynamics*, *39*(9), 3213–3212.

Jaillet, L., Artemova, S., & Redon, S. (2017). IM-UFF: Extending the universal force field for interactive molecular modeling. *Journal of Molecular Graphics & Modelling*, *77*, 350–362.

Jean, B. M., Nâg-Tiero, M. R., Hermann, O. Y., & Germaine, N. O. (2019). Traditional uses, phytochemistry and pharmacology review of 2 Vitex: Diversifolia and doniana. *International Journal of Research and Development in Pharmacy & Life Sciences*, *8*(2), 29–36. https://doi.org/10.21276/IJRDPL.2278-0238.2019.8(2).29-36

Kadioglu, O., Saeed, M., Greten, H. J., & Efferth, T. (2021). Identification of novel compounds against three targets of SARS CoV-2 coronavirus by combined virtual screening and supervised machine learning. *Computers in biology and medicine*, *133*, 104359.

Khan, T., Khan, M. A., Ullah, N., & Nadhman, A. (2020). Therapeutic potential of medicinal plants against COVID-19: The role of antiviral medicinal metabolites. *Biocatalysis and Agricultural Biotechnology*, *31*, 101890.

Kim, S., Chen, J., Cheng, T., Gindulyte, A., He, J., He, S., Li, Q., Shoemaker, B. A., Thiessen, P. A., Yu, B., Zaslavsky, L., Zhang, J., & Bolton, E. E. (2019). PubChem 2019 update: Improved access to chemical data. *Nucleic Acids Research*, *47*(D1), D1102–D1109. https://doi.org/10.1093/nar/gky1033

Kumari, R., Kumar, R., Lynn, A, & Open Source Drug Discovery Consortium. (2014). g_mmpbsa-a GROMACS tool for high-throughput MM-PBSA calculations. *Journal of Chemical Information and Modeling*, *54*(7), 1951–1962. https://doi.org/10.1021/ci500020m

Kwofie, S. K., Broni, E., Asiedu, S. O., Kwarko, G. B., Dankwa, B., Enninful, K. S., Tiburu, E. K., & Wilson, M. D. (2021). Cheminformatics-based identification of potential novel anti-SARS-CoV-2 natural compounds of African origin. *Molecules*, *26*(2), 406. https://doi.org/10.3390/molecules26020406

Kwofie, S. K., Broni, E., Teye, J., Quansah, E., Issah, I., Wilson, M. D., Miller, W. A., Tiburu, E. K., & Bonney, J. H. K. (2019). Pharmacoinformatics-based identification of potential bioactive compounds against Ebola virus protein VP24. *Computers in Biology and Medicine*, *113*, 103414. https://doi.org/10.1016/j.compbiomed.2019.103414

Kwofie, S. K., Dankwa, B., Enninful, K. S., Adobor, C., Broni, E., Ntiamoah, A., & Wilson, M. D. (2019). Molecular docking and dynamics simulation studies predict munc18b as a target of mycolactone: A plausible mechanism for granule exocytosis impairment in Buruli Ulcer Pathogenesis. *Toxins*, *11*(3), 181. https://doi.org/10.3390/toxins11030181

Kwofie, S. K., Enninful, K. S., Yussif, J. A., Asante, L. A., Adjei, M., Kan-Dapaah, K., Tiburu, E. K., Mensah, W. A., Miller, W. A., Mosi, L., &

Wilson, M. D. (2019). Molecular informatics studies of the iron-dependent regulator (ideR) reveal potential novel anti-mycobacterium ulcerans natural product-derived compounds. *Molecules*, *24*(12), 2299. https://doi.org/10.3390/molecules24122299

Lagunin, A., Stepanchikova, A., Filimonov, D., & Poroikov, V. (2000). PASS: Prediction of activity spectra for biologically active substances. *Bioinformatics (Oxford, England)*, *16*(8), 747–748.

Laskowski, R. A., & Swindells, M. B. (2011). LigPlot+: multiple ligand-protein interaction diagrams for drug discovery. *Journal of Chemical Information and Modeling*, *51*(10), 2778–2786. https://doi.org/10.1021/ci200227u

Leakey, R. R. (2001). Win: Win landuse strategies for Africa: 1. Building on experience with agroforests in Asia and Latin America. *The International Forestry Review*, 1–10.

Lemkul, J. (2019). From proteins to perturbed Hamiltonians: A suite of tutorials for the GROMACS-2018 molecular simulation package [article v1. 0]. *Living Journal of Computational Molecular Science*, *1*(1), 5068.

Li, W., Xu, C., Hao, C., Zhang, Y., Wang, Z., Wang, S., & Wang, W. (2020). Inhibition of herpes simplex virus by myricetin through targeting viral gD protein and cellular EGFR/PI3K/Akt pathway. *Antiviral Research*, *177*, 104714.

Lipinski, C. A. (2016). Rule of five in 2015 and beyond: Target and ligand structural limitations, ligand chemistry structure and drug discovery project decisions. *Advanced Drug Delivery Reviews*, *101*, 34–41. https://doi.org/10.1016/j.addr.2016.04.029

Mandrekar, J. N. (2010). Receiver operating characteristic curve in diagnostic test assessment. *Journal of Thoracic Oncology : Official Publication of the International Association for the Study of Lung Cancer*, *5*(9), 1315–1316. https://doi.org/10.1097/JTO.0b013e3181ec173d

Marin, M., Watson, T. L., Chaves, S. S., Civen, R., Watson, B. M., Zhang, J. X., Perella, D., Mascola, L., & Seward, J. F. (2008). Varicella among adults: Data from an active surveillance project, 1995–2005. *The Journal of Infectious Diseases*, *197*(s2), S94–S100. https://doi.org/10.1086/522155

Martin, Y. C. (2005). A bioavailabilty score. *Journal of Medicinal Chemistry*, *48*(9), 3164–3170. ACS Publications), https://doi.org/10.1021/jm0492002

Migliore, M. (2010). FV-100: The most potent and selective anti-varicella zoster virus agent reported to date. *Antiviral Chemistry and Chemotherapy*, *20*(3), 107–115. https://doi.org/10.3851/IMP1472

Minai-Tehrani, D., Soheili, Z., & Yahyavi, E. (2015). Inhibition of microbial alkaline phosphatase by cimetidine; kinetics and molecular model of binding. *Current Enzyme Inhibition*, *11*(1), 39–45. https://doi.org/10.2174/1573408011666150226231233

Mothana, R. A. A., Abdo, S. A. A., Hasson, S., Althawab, F. M. N., Alaghbari, S. A. Z., & Lindequist, U. (2010). Antimicrobial, antioxidant and cytotoxic activities and phytochemical screening of some yenemi medicinal plants. *Evidence-Based Complementary and Alternative Medicine : eCAM*, *7*(3), 323–330.

Mysinger, M. M., Carchia, M., Irwin, J. J., & Shoichet, B. K. (2012). Directory of useful decoys, enhanced (DUD-E): better ligands and decoys for better benchmarking. *Journal of Medicinal Chemistry*, *55*(14), 6582–6594.

Osuagwu, G., & Eme, C. (2013). The phytochemical composition and antimicrobial activity of Dialium guineense, Vitex doniana and Dennettia tripetala leaves. *Asian Journal of Natural Applied Sciences*, *2*(3), 69–81.

Park, C. S., Kim, D. S. S., & Kim, K. H. (2013). Varicella outbreak in the patients during group therapy: Seroprevalence in a Healthcare system during breakthrough varicella occurrence. *Clinical and Experimental Vaccine Research*, *2*(2), 140–143. https://doi.org/10.7774/cevr.2013.2.2.140

Peele, K. A., Potla Durthi, C., Srihansa, T., Krupanidhi, S., Ayyagari, V. S., Babu, D. J., Indira, M., Reddy, A. R., & Venkateswarulu, T. C. (2020). Molecular docking and dynamic simulations for antiviral compounds against SARS-CoV-2: A computational study. *Informatics in Medicine Unlocked*, *19*, 100345. https://doi.org/10.1016/j.imu.2020.100345

Pires, D. E., Blundell, T. L., & Ascher, D. B. (2015). pkCSM: Predicting small-molecule pharmacokinetic and toxicity properties using graph-based signatures. *Journal of Medicinal Chemistry*, *58*(9), 4066–4072.

Prasanth, D., Murahari, M., Chandramohan, V., Panda, S. P., Atmakuri, L. R., & Guntupalli, C. (2020). In silico identification of potential inhibitors from Cinnamon against main protease and spike glycoprotein of SARS CoV-2. *Journal of Biomolecular Structure and Dynamics*, *39*, 1–15.

Sang, H., Huang, Y., Tian, Y., Liu, M., Chen, L., Li, L., Liu, S., & Yang, J. (2021). Multiple modes of action of myricetin in influenza A virus infection. *Phytotherapy Research*, *35*(5), 2797-2806. https://doi.org/10.1002/ptr.7025

Schrodinger, L. (2010). The PyMOL molecular graphics system. *Version*, *1*(5), 0.

Schüttelkopf, A. W., & Van Aalten, D. M. (2004). PRODRG: A tool for high-throughput crystallography of protein–ligand complexes. *Acta Crystallographica Section D Biological Crystallography*, *60*(8), 1355–1363. https://doi.org/10.1107/S0907444904011679

Selick, H. E., Beresford, A. P., & Tarbit, M. H. (2002). The emerging importance of predictive ADME simulation in drug discovery. *Drug Discovery Today*, *7*(2), 109–116.

Sharma, A., Cooper, R., Bhardwaj, G., & Cannoo, D. S. (2021). The Genus Nepeta: Traditional uses, phytochemicals and pharmacological properties. *Journal of Ethnopharmacology*, *268*, 113679.

Singh, M., Chandran, C., Sarwa, A., Kumar, A., Gupta, M., Raj, A., & Ratho, R. (2015). Outbreak of chickenpox in a Union Territory of North India. *Indian Journal of Medical Microbiology*, *33*(4), 524–527. https://doi.org/10.4103/0255-0857.167335

Spadola, L., Novellino, E., Folkers, G., & Scapozza, L. (2003). Homology modelling and docking studies on Varicella Zoster Virus Thymidine kinase. *European Journal of Medicinal Chemistry*, *38*(4), 413–419.

Stilinović, V., Horvat, G., Hrenar, T., Nemec, V., & Cinčić, D. (2017). Halogen and hydrogen bonding between (N-halogeno)-succinimides and pyridine derivatives in solution, the solid state and in silico. *Chemistry - A European Journal*, *23*(22), 5244–5257. https://doi.org/10.1002/chem.201605686

Topalis, D., Gillemot, S., Snoeck, R., & Andrei, G. (2018). Thymidine kinase and protein kinase in drug-resistant herpesviruses: Heads of a Lernaean Hydra. *Drug Resistance Updates: Reviews and Commentaries in Antimicrobial and Anticancer Chemotherapy*, *37*, 1–16.

Tort, A. (2013). A note on the electrostatic energy of two point charges. *arXiv preprint arXiv:*.

Trott, O., & Olson, A. (2010). AutoDock Vina: Improving the speed and accuracy of docking with a new scoring function, efficient optimization, and multithreading. *Journal of Computational Chemistry*, *31*(2), 455–461.

Turner, P. (2005). *XMGRACE, version 5.1. 19*. Center for Coastal and Land-Margin Research, Oregon Graduate Institute of Science and Technology.

Veber, D. F., Johnson, S. R., Cheng, H.-Y., Smith, B. R., Ward, K. W., & Kopple, K. D. (2002). Molecular properties that influence the oral bioavailability of drug candidates. *Journal of Medicinal Chemistry*, *45*(12), 2615–2623. https://doi.org/10.1021/jm020017n

Wallace, A. C., Laskowski, R. A., & Thornton, J. M. (1995). LIGPLOT: A program to generate schematic diagrams of protein-ligand interactions. *Protein Engineering*, *8*(2), 127–134. https://doi.org/10.1093/protein/8.2.127

Wang, N., Chen, W., Zhu, L., Zhu, D., Feng, R., Wang, J., Zhu, B., Zhang, X., Chen, X., Liu, X., Yan, R., Ni, D., Zhou, G. G., Liu, H., Rao, Z., & Wang, X. (2020). Structures of the portal vertex reveal essential protein-protein interactions for Herpesvirus assembly and maturation. *Protein & Cell*, *11*(5), 366–373. https://doi.org/10.1007/s13238-020-00711-z

World Health Organization. (2002). *The world health report 2002: reducing risks, promoting healthy life*. World Health Organization.

Yaeghoobi, M., Frimayanti, N., Chee, C. F., Ikram, K. K., Najjar, B. O., Zain, S. M., Abdullah, Z., Wahab, H. A., & Rahman, N. A. (2016). QSAR, in silico docking and in vitro evaluation of chalcone derivatives as potential inhibitors for H1N1 virus neuraminidase. *Medicinal Chemistry Research*, *25*(10), 2133–2142. https://doi.org/10.1007/s00044-016-1636-5

Yu, M.-S., Lee, J., Lee, J. M., Kim, Y., Chin, Y.-W., Jee, J.-G., Keum, Y.-S., & Jeong, Y.-J. (2012). Identification of myricetin and scutellarein as novel chemical inhibitors of the SARS coronavirus helicase, nsP13. *Bioorganic & Medicinal Chemistry Letters*, *22*(12), 4049–4054. https://doi.org/10.1016/j.bmcl.2012.04.081